

LASER BIOLOGY

PACS numbers: 07.60.Dq; 87.64.–t; 87.57.C–
DOI: 10.1070/QE2008v038n03ABEH013598

Visualisation of the distributions of melanin and indocyanine green in biological tissues

E.A. Genina, I.V. Fedosov, A.N. Bashkatov,
D.A. Zimnyakov, G.B. Altshuler, V.V. Tuchin

Abstract. **A double-wavelength laser scanning microphotometer with the high spectral and spatial resolutions is developed for studying the distribution of endogenic and exogenic dyes in biological tissues. Samples of hair and skin biopsy with hair follicles stained with indocyanine green are studied. The spatial distribution of indocyanine green and melanin in the biological tissue is determined from the measured optical transmittance.**

Keywords: *visualisation, double-wavelength laser scanning microphotometer, melanin, indocyanine green.*

1. Introduction

Lasers find expanding applications in medicine and cosmetology. Along with the rapid development of diagnostic methods such as optical coherent tomography [1], laser fluorescence spectroscopy [2], confocal and multiphoton fluorescence microscopy [3, 4], new technologies in laser therapy and surgery attract the attention of researchers. Among them are the photodynamic therapy of cancer [5] and infectious diseases [6], laser photothermolysis in medical treatment of acne vulgaris [7] and other dermatology diseases [8], laser photothermolysis in conjunction with local immunotherapy of cancer tumours [9], coagulation of blood vessels [10], laser eye surgery [11], laser correction of cartilaginous tissues [12], hair depilation [13], etc.

To enhance the image contrast of objects under study in laser diagnostics and to produce the selective laser action on biological tissues, both endogenic and exogenic chromophores are used. They include melanin, haemoglobin, porphyrins, and photosensitisers and biologically compatible dyes having a sufficiently narrow absorption band in the 'therapeutic window' region between 600 and 1200 nm, i.e. in the wavelength range where the intrinsic absorption of biological tissues is comparatively weak. The use of these dyes requires a detailed study of their localisation regions and distributions in biological tissues. Despite numerous studies devoted to this problem, the investigation of the localisation of dyes in biological tissues remains an urgent problem. For this purpose, various optical methods are used, in particular, Raman spectroscopy [14], confocal microscopy [4, 15], reflection spectroscopy [16, 17], fluorescence spectroscopy [18, 19], photoacoustic methods [17], the digital analysis of optical images [20 – 23], and others.

Indocyanine green (ICG), a biologically compatible dye having the intense absorption band in the near-IR region at $\sim$800 nm and a weaker band at $\sim$720 nm, is widely used both for fluorescence diagnostics of the functions of liver, kidneys, heart [24, 25], brain blood circulation [26, 27], and the localisation of tumours [28, 29] by visualising blood streams in blood vessels feeding a tumour. The possibility of using ICG as a photosensitiser in photodynamic therapy was demonstrated in many papers [7, 30]. The narrow absorption band and the high absorption coefficient of this dye allow its applications in photothermal therapy [7, 9] and laser photocoagulation and welding of biological tissues [11, 31]. Depending on a solvent and the ICG concentration in the solution, its absorption maximum can vary between 650 and 820 nm; this also occurs during the bonding of the dye with biological molecules in cells [30, 32 – 34]. Laser excitation into the absorption band of ICG provides the high selectivity of the combined action of the laser and dye, excluding the damage of the healthy tissue. In this case, it is important to know the distribution of the dye in a biological tissue to provide the optimal dose and localisation of laser radiation.

The visualisation of ICG in the skin by fluorescence spectra requires the use of the expensive equipment [24 – 28]. In addition, to monitor simultaneously the content of melanin and ICG in the skin, microspectrophotometry should be performed in a broad spectral range. The visualisation method based on the digital analysis of the colour images of the skin has received wide applications due to its availability and a comparatively low cost [20 – 23]. The information content and contrast of images are enhanced by means of polarisation filters, which either improve the quality of observation of the surface properties of the skin or allow the observation of processes proceeding under the skin surface such as erythema and pigmentation or of hair follicles, etc. However, this method often gives only estimates.

Thus, the problem of visualisation and localisation of endogenic and exogenic dyes in biological tissues remains topical. The aim of this paper is to develop a device for the

E.A. Genina, I.V. Fedosov, A.N. Bashkatov, D.A. Zimnyakov, V.V. Tuchin Institute of Optics and Biophotonics, N.G. Chernyshevsky Saratov State University, ul. Astrakhanskaya 83, 410012 Saratov, Russia;
e-mail: eagenina@optics.sgu.ru, zimnykov@sgu.ru;
G.B. Altshuler Palomar Medical Technology Inc., 82, Cambridge St., Burlington 01803, USA

Received 20 April 2007; revision received 13 July 2007
Kvantovaya Elektronika **38** (3) 263 – 268 (2008)
Translated by M.N. Sapozhnikov

simultaneous visualisation of melanin and indocyanine green in the skin.

2. Methods and materials

The experimental setup is based on a standard universal binocular 60× microscope (Fig. 1). Laser radiation was focused by the objective of the microscope condenser in a spot of diameter 2–10 μm on a sample. The sample was placed in an immersion liquid with the refractive index $n = 1.5$ between the object and cover glasses, which were fixed on a translation stage. The stage translations were performed in the mutually perpendicular directions in the horizontal plane with a step of 10 μm by means of two computer-controlled step motors. Measurements were performed with the help of an Abbe refractometer at 589 nm for $t = 20$ °C.

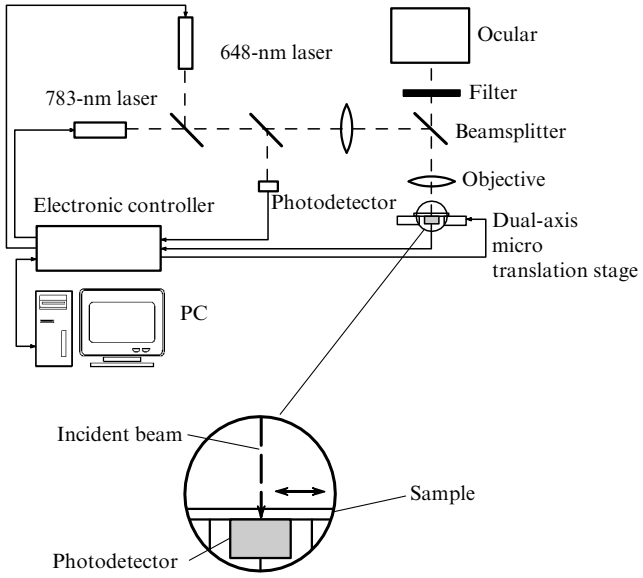

Figure 1. Scheme of a two-wavelength laser scanning microphotometer.

The transmittance of biological tissues was measured with two photodetectors. The incident beam intensity was measured by deflecting a part of the beam by means of a thin glass beamsplitter in the receiving channel of the reference photodetector. The measuring photodetector with the photodiode area of 3 × 3 mm was placed directly at a distance of 1.5 mm under the sample and collected the scattered light within a wide angular aperture ~45°, which was determined by the photodetector parameters. Signals from each of the photodiodes were amplified, digitised in an ADC (L-154, L-card, Russia), and fed to a PC. Two pulsed 648-nm and 783-nm diode lasers were used as radiation sources. These wavelengths are used because the absorption maximum of the ICG solution is located at 783 nm and absorption in the dye solution in this region exceeds absorption by melanin contained in human hairs, whereas absorption in melanin at 648 nm, on the contrary, dominated over absorption in the ICG solution. The spectral dependences of the optical density of the ICG solution [32] and human hairs [35] are shown in Fig. 2.

Lasers generated alternately the trains of ten 1-ms pulses with a pulse repetition period of 2 ms. Simultaneously with

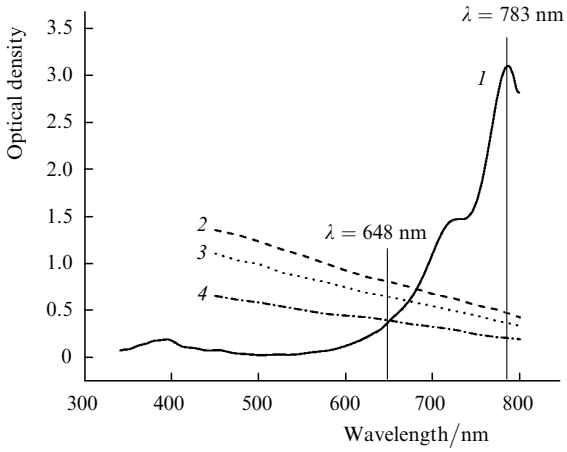

Figure 2. Spectral dependences of the optical density of the ICG solution (*1*) and dark brown (*2*), brown (*3*), and light yellow-brown (*4*) hairs [35].

the generation of pulses, the output signals of photodetectors were fed via the ADC to the PC. The transmittance of the sample at each point was determined as the ratio of signals from the measuring and reference photodiodes. This allowed us to take into account the fluctuations of the photodiode power during measurements.

To minimise the influence of scattering in biological tissues, the refractive indices of the biological tissue and environment were matched by immersion to exclude the scattering of light from the sample surface. The light transmitted through the sample was collected within a wide angular aperture. The measurement system was calibrated by a signal from glasses with immersion liquid between them. This procedure allowed us to take into account signal losses due to absorption of radiation in the glass and immersion liquid and reflection of radiation from the air–glass–immersion liquid–glass–air interfaces.

The transmittance of biological tissues was measured with the microphotometer at two wavelengths. The spatial resolution of the microphotometer in the study of hairs was ~20 μm along the hair stem and 10 μm across it. The transmittance distribution was obtained by scanning a laser beam 30 times across the hair stem, the transmittance at each point being determined from averaged transmittances obtained in each transverse scanning.

The scan area and step were chosen depending on the sample size. The two-dimensional array of the transmittance values of the sample at 648 and 783 nm was recorded during the scan.

The visualisation method of the ICG dye distribution regions in skin samples includes several stages:

(i) The object is imaged at 648 nm and 783 nm based on the scan data. The brightness B of each of the image pixels, varying between 0 and 255, is matched to the transmitted radiation intensity. Thus, the white colour, having the highest brightness 255, is assigned to the maximum transmitted radiation intensity, while the black colour, having the brightness 0, corresponds to the zero signal.

(ii) The difference image is determined by subtracting the transmitted radiation intensity at 783 nm from that at 648 nm. Because absorption in ICG at 783 nm exceeds its absorption at 648 nm, and therefore the transmission of light in stained regions at 648 nm considerably exceeds their transmission at 783 nm, the stained regions have positive

intensity differences. For melanin, on the contrary, transmission at 648 nm is smaller than at 783 nm, and therefore the intensity differences in the regions containing melanin will be negative. (Upon visualisation of melanin localisation regions, the difference image is obtained by subtracting the radiation intensities obtained at 648 nm from those obtained at 783 nm. In this case, only regions containing melanin will have positive intensity differences.) The image is constructed in the grey-level scale, the white colour being assigned to the maximum intensity difference and the black colour – to the minimum intensity difference.

(iii) To visualise the dye more distinctly, a contrast image is constructed by assigning zero values to the negative intensities in the difference image and representing them by the black colour in the image, while the grey shades are assigned only to positive intensity values. Thus, only regions stained by ICG remain in the image, which enhances the image contrast.

This system is adjusted to each image of a biological tissue, by assigning the white colour to the maximum intensity to enhance the image contrast.

We studied the distribution of melanin and ICG in the skin *in vitro* by using seven skin biopsy samples from volunteers, which was preliminarily stained *in vivo* by the ICG solution (Palomar Medical Product Inc., USA) [32]. The solvent contained glycerol, propylene glycol, ethanol, and water, which provided the better penetration of the dye to the skin. The absorption maximum of the solution was located at 783 nm. The skin biopsy was performed from the external region of the forearm of two healthy volunteers by means of special instruments for biopsy (Acuderm Inc., USA) in a clinic by the standard method using the local anaesthesia. The skin with dark hairs was studied. The samples were 2 mm in diameter and 4 – 5 mm in depth.

All the samples were additionally photographed with a microscopic video system combined with a PC.

3. Results and discussion

Figure 3 demonstrates the measured optical transmittance of an individual unstained hair and the hair image constructed based on it. The transmittance distribution along the hair axis is shown in Fig. 3a. The measurement error of the average transmittance was 5 %. One can see that the transmittance at 648 nm is considerably lower than that at 783 nm. This is explained by the absorption in melanin contained in hair. The absorption spectrum of melanin has no distinct absorption bands and the absorption coefficients of the two types of melanin – eumelanin and pheomelanin, monotonically decrease with increasing wavelength from 200 to 1100 nm [36, 37]. Absorption in melanin in the near-IR region becomes negligible.

Figures 3b and c present the hair images at two wavelengths. The lighter image in Fig. 3c corresponds to the transmittance distribution for the hair at 783 nm, and the darker image in Fig. 3b – to that at 648 nm. The images exhibit distinct dark regions with the higher amount of melanin in the hair bulb and stem, which are inherent in the growing hair. In the hair bulb, the functioning melanocytes – cells producing melanosomas – are located; here, melanin is also released from melanosomes. Afterwards, melanin granules are fixed between keratin fibrils during the hair growth and densification, thereby distributing over the hair stem. The mitotic activity of melanocytes, the production of melanosomes and their release to the hair stem occur only in the active phase of the hair cycle [38].

Figure 4 demonstrates the stages of receiving a contrast image. Figure 4a presents the microphotograph of the fragment of the epilated hair in the follicle region. The

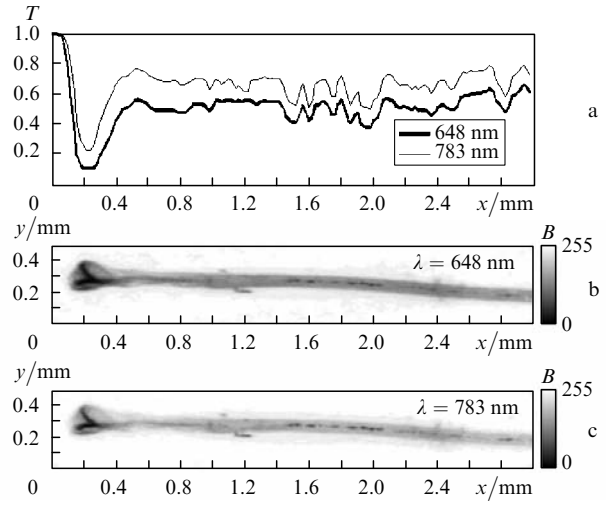

Figure 3. Distribution of the transmittance T of the hair along its axis (a) and hair images constructed by its transmittances at 648 nm (b) and 783 nm (c).

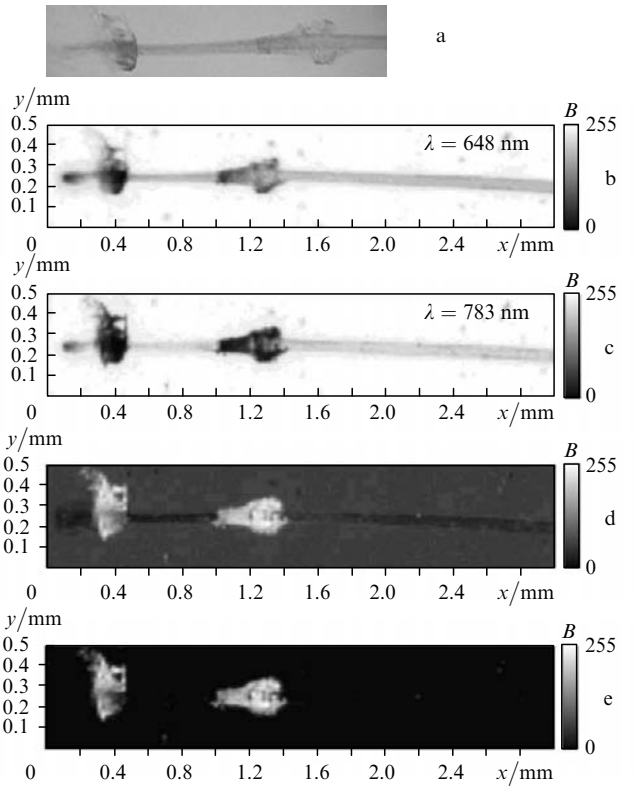

Figure 4. Images of the hair fragment stained *in vivo* by the ICG solution: microphotography obtained by using a microscopic video system (a); images of the hair constructed by its transmittances at 648 nm (b) and 783 nm (c); the hair image constructed by the difference of intensities at 648 and 783 nm (d) and the contrast image of the hair constructed by the positive difference intensity at 648 and 783 nm (e).

hair was epilated from the skin on which the ICG solution was applied. This image obtained with the help of a microscopic video system shows the stained follicle regions; however, the accurate determination of the depth and boundary of the stained regions is complicated. Figures 4b and c show the hair images constructed by the values of the hair transmittance at 648 and 783 nm. One can see that the follicle regions stained with ICG are darker in Fig. 4c than in Fig. 4b because absorption of ICG at 783 nm exceeds its absorption at 648 nm. For melanin, on the contrary, transmission at 648 nm is smaller than at 783 nm, and therefore the hair stem in Fig. 4b looks darker than in Fig. 4c. Thus, after the subtraction of the intensity values at 783 nm from these at 648 nm, only the region stained with ICG have positive intensity values. The difference hair image is shown in Fig. 4d. The distribution boundaries of the dye in the tissue can be determined more accurately by distinguishing the region with positive intensity values by the grey shades and representing the rest of the region in the black colour, thereby considerably increasing the image contrast. The contrast image of the hair is presented in Fig. 4e.

To distinguish clearly the dye localisation regions and to determine accurately the boundaries of the dye distribution in the skin stained with the ICG solution is even more difficult than in an individual hair because the dye concentration in follicles is low and light is strongly scattered in the skin. The ICG distribution in the skin obtained by the method proposed here is shown in Fig. 5, where the microphotograph of the fragment of the skin biopsy with two hair follicles is presented. The ICG solution was preliminarily applied on and rubbed in the skin of a volunteer, the remaining solution being then removed. Because the skin biopsy sample was a cone with the apex located deep in the skin and the base located on the skin surface, when the sample was covered with a cover glass, the stained skin surface occupied the region of width ~ 0.2 mm in the upper part of the sample (the dark strip at the left edge of the sample in Fig. 5a). The dye was also distributed along follicles and accumulated in the region of the oil gland output at a depth of $0.2-0.3$ mm under the skin. The stained regions in Fig. 5a look darker; however, it is impossible to determine the boundaries of the dye distribution region. The difference images of each of the follicles shown in Figs. 5b and c allow us to refine the penetration depth of ICG inside follicles, which proved to be equal to 0.93 ± 0.02 and 0.59 ± 0.02 mm, respectively. The spatial double-wavelength scanning and processing of the obtained images give the distinct localisation regions of melanin (dark regions) in hair follicles and of ICG on the skin surface and along hair follicles. Thus, the difference image of the skin sample proves to be considerably more informative than microphotographs.

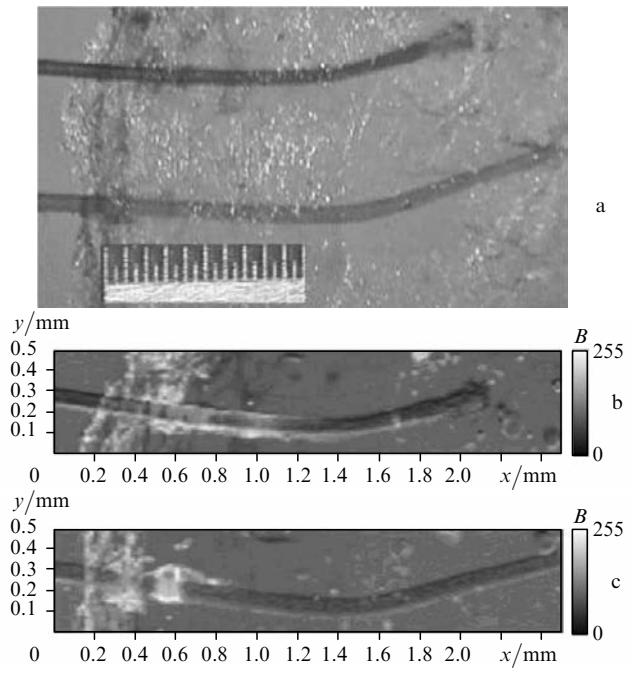

Figure 5. Image of the fragment of the skin biopsy with hairs stained *in vivo* by the ICG solution; microphotograph obtained with the help of a microscopic video system (a) and the contrast images of the upper (b) and lower (c) hair.

There exist methods for visualisation of dyes in biological tissues such as scanning confocal and fluorescence microscopy and multiphoton microscopy which have a better resolution achieving $1-3$ μm [4, 15]; however, they require the expensive instruments. The digital image analysis provides quite accurate visualisation of the stained regions of biological tissues with distinctly outlined boundaries [21, 22]. However, at low dye concentrations, when the colours of the stained and unstained regions of a biological tissue differ insignificantly or the boundaries of the stained region are blurred, this method cannot provide reliable results.

The spatial resolution of the method of double-wavelength laser scanning depends first of all on the geometrical parameters of the probe laser beam. The choice of these parameters is determined to a great extent by the sample thickness because the beam cross section should not change significantly over the sample thickness. We used here skin samples of thickness from 30 to 70 μm (hairs) and from100 to 200 μm (skin biopsy samples). To provide the constant cross section of the laser beam over the sample thickness, laser radiation was focused with a waist of diameter ~ 10 μm. Because the main scatterers in the hair are keratinocytes, melanocytes, and air bubbles of micron and submicron sizes, according to the Mie theory, the indicatrix of radiation transmitted through the sample is strongly anisotropic, the main part of radiation being scattered forward. The use of a wide-aperture photodetector eliminates the influence of scattering of light by biological tissues on the estimate of absorption. Moreover, the application of the immersion liquid considerably reduces light scattering and enhances the intensity of the directly propagated radiation component [39]. The geometrical parameters of the scheme used in experiments were calculated based on the optical thickness of the hair of the order of $4-5$, which were obtained from the data presented in [23]. In the case of thinner samples, a tighter focusing is possible, which can provide the spatial resolution of a scanning microphotometer to 1.5 μm.

The refractive index $n = 1.5$ of immersion liquid used in experiments can be considered constant in the range from 580 to 800 nm [40]. The immersion agent, which has the refractive index close to that of the main scatterers (collagenic fibres) in the skin, $n_{\mathrm{col}} = 1.47$ [39], considerably affects the scattering properties of the skin, by reducing the

scattering coefficient due to matching between the refractive indices of the tissue fluid and collagenic fibres [39]. The refractive index of keratinocytes (basic components of hairs) is 1.5 [41], and for this reason the immersion agent reduces by tens of times scattering from the hair surface caused by its inhomogeneities. As shown in [23], dark hairs containing melanin at high concentrations have comparatively weak scattering parameters compared to hairs of other types [$\mu_s' \sim 30$ and ~ 15 cm^{-1} at 648 and 783 nm, respectively, where $\mu_s' = \mu_s(1-g)$ is the transport scattering coefficient; μ_s is the scattering coefficient; and g is the anisotropy factor], which is obviously related to the size of scatterers in these hairs and their dense packing. Due to the use of immersion, the intensity of transmitted radiation will be mainly determined by the absorption of light by the structural components of biological tissues. However, melanin, having the refractive index equal to 1.7 [42], will still contribute to light scattering, which will lead to the additional increase in the image contrast upon visualisation of the melanin distribution. At the same time, the influence of immersion on the absorbing properties of biological tissues can be considered insignificant [39]. Thus, the immersion liquid does not distort considerably the visualisation of the distribution of dyes and pigments in biological tissues.

Other factors determining the spatial resolution are the accuracy of the sample positioning and the recording time of one point of the image. In the case of fast scanning devices, it is possible to study extended samples with a very high resolution because the dimensions of the sample are restricted only by the maximum travel of a dual-axis translation stage. Thus, the maximum travel of the translation stage in our system was 100 mm with an error of 10 μm, which allows the study of tissue samples of size greatly exceeding the field of view of a standard microscope.

Thus, the method of spatial two-wavelength laser scanning and image processing is quite simple to realise and can be used for studying the diffusion of dyes in biological tissues and measuring the boundaries of localisation regions of melanin and dyes in various biological structures.

4. Conclusions

By using the two-wavelength laser scanning, we have determined quire accurately the spatial distribution of the transmittance of biological tissues at two wavelengths and constructed the difference image separating with a high contrast the localisation regions of melanin and the dye in the biological tissue.

The main advantage of this method is its low sensitivity to the small-angle scattering loss of the probe radiation because the aperture of a photodetector provides the collection of the greater part of forward-scattered radiation.

The scanning microphotometer described in the paper and the method for obtaining the images of biological tissues can be used in medicine and biology, in particular, for optical diagnostics, photodynamic and laser therapy, and the study of distributions of natural pigments and some organic dyes, in particular, indocyanine green in biological structures.

Acknowledgements. This work was supported by Palomar Medical Technologies Inc. (Burlington, USA), the U.S. Civilian Research & Development Foundation for the Independent States of the Former Soviet Union (Grant Nos REC-006 and PG05-006-2), and the Russian Foundation for Basic Research (Grant No. 06-02-16740).

References

1. Moger J., Matcher S.J., Winlove C.P., Shore A. *J. Phys. D: Appl. Phys.*, **38**, 2597 (2005).
2. Zhu B., Jaffer F., Ntziachristos V., Weissleder R. *J. Phys. D: Appl. Phys.*, **38**, 2701 (2005).
3. Gerger A., Koller S., Kern T., Massone C., Steiger K., Richtig E., Kerl H., Smolle J. *J. Invest. Dermatol.*, **124**, 493 (2005).
4. Masters B.R., So P.T.C. *Opt. Express*, **8**, 2 (2001).
5. Stranadko E.F., Ivanov A.V. *Biofizika*, **49**, 380 (2004).
6. Genina E.A., Bashkatov A.N., Chikina E.E., Knyazev A.B., Mareev O.V., Tuchin V.V. *Laser Phys.*, **16**, 1128 (2006).
7. Tuchin V.V., Genina E.A., Bashkatov A.N., Simonenko G.V., Odoevskaya O.D., Altshuler G.B. *Lasers Surg. Med.*, **33**, 296 (2003).
8. Ackermann G., Hartmann M., Scherer K., Lang E.W., Hohenleutner U., Landthaler M., Baumler W. *Lasers Med. Sci.*, **17**, 70 (2002).
9. Chen W.R., Liu H., Carubelli R., Nordquist R.E. *J. X-Ray Sci. Technol.*, **10**, 225 (2002).
10. Dai T., Diagaradjane P., Yaseen M.A., Pikkula B.M., Thomsen S., Anvari B. *Lasers Surg. Med.*, **37**, 210 (2005).
11. Kuo P.-Ch., Peyman G.A., Men G., Bezerra Y., Torres F. *Lasers Surg. Med.*, **35**, 157 (2004).
12. Zuger B.J., Ott B., Mainil-Varlet P., Schaffner Th., Clemence J.-F., Weber H.P., Frenz M. *Lasers Surg. Med.*, **28**, 427 (2001).
13. Campos V.B., Dierickx C.C., Farinelli W.A., Lin T.-Y.D., Manuskiatti W., Anderson R.R. *Lasers Surg. Med.*, **26**, 177 (2000).
14. Huang Z., Lui H., Chen X.K., Alajlan A., McLean D.I., Zeng H. *J. Biomed. Opt.*, **9**, 1198 (2004).
15. Rajadhyaksha M., Grossman M., Esterrowitz D., Webb R.H., Anderson R.R. *J. Invest. Dermatol.*, **104**, 946 (1995).
16. Stamatas G.N., Zmudzka B.Z., Kollias N., Beer J.Z. *Pigment Cell Res.*, **17**, 618 (2004).
17. Viator J.A., Komadina J., Svaasand L.O., Aguilar G., Choi B., Nelson J.S. *J. Invest. Dermatol.*, **122**, 1432 (2004).
18. Juzenas P., Iani V., Bagdonas S., Rotomskis R., Moan J. *J. Photochem. Photobiol. B.*, **61**, 78 (2001).
19. Andrejevic-Blant S., Major A., Ludicke F., Ballini J.-P., Wagnieres G., van den Bergh H., Pelte M.-F. *Lasers Surg. Med.*, **35**, 276 (2004).
20. Takamoto T., Schwartz B., Cantor L.B., Hoop J.S., Steffens T. *Current Eye Res.*, **22**, 412 (2001).
21. Miyamoto K., Takiwaki H., Hillebrand G.G., Arase S. *Skin Res. Technol.*, **8**, 227 (2002).
22. Faziloglu Y., Stanley R.J., Moss R.H., van Stoecker W., McLean R.P. *Skin Res. Technol.*, **9**, 147 (2003).
23. Bashkatov A.N., Genina E.A., Kochubei V.I., Tuchin V.V. *Kvantovaya Elektron.*, **36**, 1111 (2006) [*Quantum Electron.*, **36**, 1111 (2006)].
24. Green F.J. *The Sigma-Aldrich Handbook of Stains, Dyes and Indicators* (Milwaukee: Aldrich Chemical Company, Inc., 1990).
25. Dorshow R.B., Bugaj J.E., Burleigh B.D., Duncan J.R., Johnson M.A., Jones W.B. *J. Biomed. Opt.*, **3**, 340 (1998).
26. Springett R., Sakata Y., Delpy D.T. *Phys. Med. Biol.*, **46**, 2209 (2001).
27. Kohl-Bareis M., Obrig H., Steinbrink J., Malak J., Uludag K., Villringer A. *J. Biomed. Opt.*, **7**, 464 (2002).
28. Li X., Beauvoit B., White R., Nioka S., Chance B., Yodh A. *Proc. SPIE Int. Soc. Opt. Eng.*, **2389**, 789 (1995).
29. Bugaj J.E., Achilefu S., Dorshow R.B., Rajagopalan R. *J. Biomed. Opt.*, **6**, 122 (2001).
30. Abels C., Fickweiler S., Weiderer P., Baumler W., Hofstadter F., Landthaler M., Szeimies R.-M. *Arch. Dermatol. Res.*, **292**, 404 (2000).

31. Athiraman H., Wolf R.F., Bartels K.E., Shivakoti S., Liu H., Chen W.R. *J. X-Ray Sci. Technol.*, **12**, 117 (2004).
32. Genina E.A., Bashkatov A.N., Sinichkin Yu.P., Kochubey V.I., Lakodina N.A., Altshuler G.B., Tuchin V.V. *J. Biomed. Opt.*, **7**, 471 (2002).
33. Weersink R.A., Hayward J.E., Diamond K.R., Patterson M.S. *J. Photochem. Photobiol.*, **66**, 326 (1997).
34. Genina E.A., Bashkatov A.N., Kochubei V.I., Tuchin V.V., Altshuler G.B. *Pis'ma Zh. Tekh. Fiz.*, **27**, 63 (2001).
35. Nicholls E.M. *Ann. Hum. Genet. Lond.*, **32**, 15 (1968).
36. Jacques S. http://omlc.ogi.edu/spectra/melanin/index.html.
37. Menon I.A., Persad S., Haberman H.F., Kurian C.J. *J. Invest. Dermatol.*, **80**, 202 (1983).
38. Rook A., Dawber R. *Diseases of the Hair and Scalp* (Oxford: Blackwell Scientific, 1982; Moscow: Medicine, 1985).
39. Tuchin V.V. *Optical Clearing of Tissues and Blood* (Bellingham: SPIE Press, 2005) Vol. PM154.
40. Fikhman B.A. *Microbiologicheskaya refaktometriya* (Microbiological Refractometry) (Moscow: Meditsina, 1967).
41. Chan D., Schulz B., Rubhausen M., Wessel S., Wepf R. *J. Biomed. Opt.*, **11**, 014029 (2006).
42. Rajadhyaksha M., Grossman M., Esterrowitz D., Webb R.H., Anderson R.R. *J. Invest. Dermatol.*, **104**, 946 (1995).